

LETTER TO THE EDITOR

Discovery of interstellar phenalene (*c*-C₁₃H₁₀): A new piece in the chemical puzzle of PAHs in space

C. Cabezas^{1,*}, M. Agúndez¹, C. Pérez², D. Villar-Castro³, G. Molpeceres¹, D. Pérez³, A. L. Steber², R. Fuentetaja¹, B. Tercero^{4,5}, N. Marcelino^{4,5}, A. Lesarri², P. de Vicente⁵, and J. Cernicharo^{1,*}

¹ Departamento de Astrofísica Molecular, Instituto de Física Fundamental (IFF-CSIC), C/ Serrano 121, 28006 Madrid, Spain

² Departamento de Química Física y Química Inorgánica, Facultad de Ciencias-I.U. CINQUIMA, Universidad de Valladolid, 47011 Valladolid, Spain

³ Centro Singular de Investigación en Química Biolóxica e Materiais Moleculares (CiQUS) and Departamento de Química Orgánica, Universidade de Santiago de Compostela, 15782 Santiago de Compostela, Spain

⁴ Observatorio Astronómico Nacional (OAN, IGN), C/ Alfonso XII, 3, 28014 Madrid, Spain

⁵ Observatorio de Yebes, IGN, Cerro de la Palera s/n, 19141 Yebes, Guadalajara, Spain

Received 31 July 2025 / Accepted 19 August 2025

ABSTRACT

We present the discovery of the unsubstituted polycyclic aromatic hydrocarbon (PAH) phenalene (C₁₃H₁₀) in TMC-1 as part of the QUIJOTE line survey. In spite of the low dipole moment of this three-ring PAH, we managed to identify a total of 267 rotational transitions with quantum numbers J and K_a up to 34 and 14, respectively, corresponding to 71 independent frequencies. The identification of this new PAH from our survey was based on the agreement between the rotational parameters derived from the analysis of the lines and those obtained by quantum chemical calculations. Our subsequent chemical synthesis of this PAH and investigation of its laboratory microwave spectrum unequivocally support our identification. We report the column density of phenalene in TMC-1 as $(2.8 \pm 1.6) \times 10^{13} \text{ cm}^{-2}$.

Key words. astrochemistry – line: identification – ISM: molecules – ISM: individual objects: TMC-1

1. Introduction

Polycyclic aromatic hydrocarbons (PAHs) are thought to be the most common type of organic molecules in the interstellar medium (ISM), based on the strength and ubiquity of the aromatic infrared bands (AIBs) attributed to PAHs four decades ago (Léger & Puget 1984; Allamandola et al. 1985; Tielens 2008). However, no individual PAH has been identified in the interstellar medium (ISM) via AIBs. The unambiguous proof of the presence of PAHs in the ISM has been provided by radioastronomy through very sensitive line surveys. Two line surveys of the Taurus Molecular Cloud (TMC-1), GOTHAM¹ (McGuire et al. 2018), and QUIJOTE² (Cernicharo et al. 2021a) have unequivocally identified a total of ten particular PAHs, namely: 1- and 2-cyanonaphthalene (McGuire et al. 2021); indene (Cernicharo et al. 2021b; Burkhardt et al. 2021a); 2-cyanoindene (Sita et al. 2022); 1- and 5-cyanoacenaphthylene (Cernicharo et al. 2024); 1-, 2-, and 4-cyanopyrene (Wenzel et al. 2024, 2025a); and cyanocoronene (Wenzel et al. 2025b).

With the presence of PAHs confirmed in the ISM, unraveling the formation and subsequent evolution of these interstellar molecules has become a central goal for the PAH community at present. The so-called “bottom-up” mechanism has been pro-

posed to explain the in situ formation of PAHs in the cold dense clouds where they have been observed (Cernicharo et al. 2021c; Byrne et al. 2024). In this scenario, PAHs are built up from small hydrocarbons in the cold and shielded environments of dark clouds. However, the opposite pathway has also been considered, known as the “top-down” route, where small PAHs result from the fragmentation of very large multi-ringed PAHs inherited from a previous evolutionary stage (Pety et al. 2005; Zhen et al. 2014; Burkhardt et al. 2021b). Thus, much work remains to be done to fully explain the origin of PAHs in the ISM, starting with a full inventory of these species, along with reasonable constraints on their abundances.

From the ten PAHs discovered in TMC-1, only one of them is an unsubstituted PAH (i.e., indene), while the other nine species are cyano-functionalised PAHs. This is because PAHs are often highly symmetric – and when they are not symmetric, they are weakly polar at best. This fact makes them notoriously difficult (if not impossible) to detect based on their rotational fingerprints. In contrast, replacing a single hydrogen on a pure PAH with a polar functional group, such as the -CN unit, yields a surrogate with a largely increased dipole moment with respect to the non-functionalised PAH counterpart, making it much easier to detect. Nevertheless, one of the most significant results of QUIJOTE was made via the standard method of line-by-line detection, leading to the discovery of low-dipole, but very abundant pure hydrocarbons, such as vinyl acetylene (CH₂CHCCH; Cernicharo et al. 2021d), cyclopentadiene and indene (*c*-C₅H₆ and *c*-C₉H₈; Cernicharo et al. 2021b), the propargyl radical (H₂CCCH; Agúndez et al. 2021, 2022),

* Corresponding authors: carlos.cabezas@csic.es,

j.cernicharo@csic.es

¹ GBT Observations of TMC-1: Hunting Aromatic Molecules.

² Q-band Ultrasensitive Inspection Journey to the Obscure TMC-1 Environment.

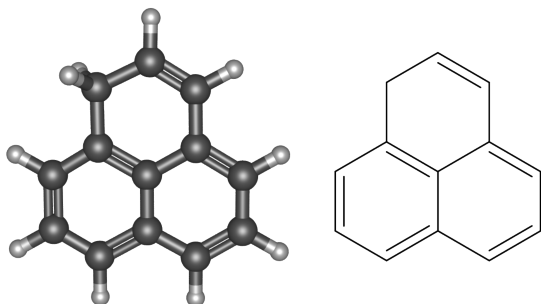


Fig. 1. 3D (left) and 2D (right) molecular structures of phenalene.

and fulvenallene ($c\text{-C}_5\text{H}_4\text{CCH}_2$; Cernicharo et al. 2022). In this Letter, we report the unequivocal detection of the second unsubstituted PAH found in space, 1*H*-phenalene (phenalene hereafter) with the molecular formula $\text{C}_{13}\text{H}_{10}$ (see Fig. 1). This low-dipole moment PAH was drawn from the QUIJOTE data and its identification was confirmed by laboratory rotational spectroscopy measurements.

2. Observations

The observations of TMC-1 reported here were acquired with the Yebes 40m telescope as part of the ongoing QUIJOTE project (Cernicharo et al. 2021a). In brief, QUIJOTE consists of a line survey in the Q band (31.0–50.3 GHz) at the position of the cyanopolyyne peak of TMC-1 ($\alpha_{J2000} = 4^{\text{h}}41^{\text{m}}41.9^{\text{s}}$ and $\delta_{J2000} = +25^{\circ}41'27.0''$). This survey was carried out using a receiver built within the Nanocosmos project³ consisting of two cooled high-electron-mobility-transistor (HEMT) amplifiers covering the Q band with horizontal and vertical polarisation. Fast Fourier transform spectrometers (FFTS) with 8×2.5 GHz and a spectral resolution of 38.15 kHz provide complete coverage of the Q band in both polarisations. The receiver temperatures are 16 K at 32 GHz and 30 K at 50 GHz. The experimental setup is described in detail in Tercero et al. (2021).

All observations are performed in the frequency-switching observing mode with a frequency throw of either 10 or 8 MHz. The total observing time on source for data taken with frequency throws of 10 MHz and 8 MHz is 772.6 and 736.6 hours, respectively. Hence, the total observing time of the QUIJOTE line survey is 1509.2 hours. The sensitivity varies between 0.06 mK at 32 GHz and 0.18 mK at 49.5 GHz. The main beam efficiency can be given across the Q band as $B_{\text{eff}} = 0.797 \exp[-(\nu(\text{GHz})/71.1)^2]$. The forward telescope efficiency is 0.97. The telescope beam size at half power intensity is $54.4''$ at 32.4 GHz and $36.4''$ at 48.4 GHz. The absolute calibration uncertainty is 10%.

The data were reduced and processed by using the CLASS package provided within the GILDAS software⁴. A detailed description of the data analysis procedure is reported in Cernicharo et al. (2022).

3. Results

Line identifications in QUIJOTE are performed using the MADEX code (Cernicharo 2012) in conjunction with the CDMS and JPL catalogues (Müller et al. 2005; Pickett et al. 1998). The intensity scale used in this study is the antenna temperature

³ <https://nanocosmos.iff.csic.es/>

⁴ <http://www.iram.fr/IRAMFR/GILDAS>

(T_A^*). Consequently, the telescope parameters and source properties were used when modelling the emission of the different species to produce synthetic spectra on this temperature scale. In this work, we assumed a velocity for the source relative to the local standard at rest of 5.83 km s^{-1} (Cernicharo et al. 2020). The source was assumed to be circular with a uniform brightness temperature and a radius of $40''$ (Fossé et al. 2001; Cernicharo et al. 2023).

Using the same methodology employed to identify the rotational transitions of the cyano derivatives of acenaphthylene (Cernicharo et al. 2024), we found several series of lines among the unknown features in the QUIJOTE line survey (see Fig. 2). We first assigned the lines in the series at higher frequencies (right side) to the a -type rotational transitions (with $K_a = 0$ and 1) $J+1_{0,J+1} \leftarrow J_{0,J}$ and $J+1_{1,J+1} \leftarrow J_{1,J}$ of a new molecular species. Then, in an iterative fitting procedure, we assigned the second series (from right to left) to the transitions with $K_a = 1$ and 2 $J+1_{1,J} \leftarrow J_{1,J-1}$ and $J+1_{2,J} \leftarrow J_{2,J-1}$. An initial fit was performed using more lines of our survey, with J and K_a values in the ranges 14–34 and 0–14, respectively. The lines were fitted using the SPFIT program (Pickett 1991) with the A -reduction of the Watson’s Hamiltonian and III^I representation (Watson 1977). From this fit, we obtained a preliminary set of molecular constants ($A = 1108.11850$, $B = 1067.81704$, and $C = 545.855894$ MHz).

From this set of rotational constants, we can infer some information on the nature of the carrier of the observed lines. First, Ray’s parameter, κ , defined as $(2B-A-C)/(A-C)$, is a way of measuring the degree of asymmetry of the molecule. For our carrier, the κ value is 0.86, which means that the molecule is a fairly oblate asymmetric rotor. Secondly, the inertial defect Δ_c , defined as $I_c - I_b - I_a$ (I_x is the inertial moment in the x molecular axes), is $-3.5051 \text{ amu } \text{Å}^2$. This value is typical for molecules with a planar-heavy atom skeleton and two methylenic hydrogen atoms as the sole out-of-plane mass contributors (Gordy & Cook 1984). Finally, the values of the rotational constants point to a molecule with a molecular size a bit larger than that of the PAHs acenaphthene ($\text{C}_{12}\text{H}_{10}$) and acenaphthylene (C_{12}H_8) (Thorwirth et al. 2007). In principle, we can discard the possibility of a cyano derivative of a PAH since the presence of a cyano moiety in a PAH induces a prolate asymmetry in the molecular framework. Examples of some cyano-PAHs with negative values of the κ parameter are 2-cyanonaphthalene (McNaughton et al. 2018), 2-cyanopyrene (Wenzel et al. 2024) and 1-cyanoacenaphthylene (Cernicharo et al. 2024), with $\kappa = -0.90$, -0.81 , and -0.46 , respectively. Based on all these points, the first candidate to be considered a carrier of our lines is a PAH with one more carbon atom than acenaphthene and acenaphthylene. The first possibility we considered was a PAH with the molecular formula $\text{C}_{13}\text{H}_{10}$, which corresponds to the two isomers fluorene and phenalene, also known as 9*H*-fluorene and 1*H*-phenalene. Fluorene can be discarded because its rotational spectrum is already known (Thorwirth et al. 2007). In contrast, its isomer phenalene (see structure in Fig. 1) has never been observed in the laboratory. It is a promising candidate since its molecular structure appears, to some extent, oblate and displays an out-of-plane methylene $-\text{CH}_2$ moiety.

To gain some insights into the rotational constants of phenalene, we carried out quantum chemical calculations to optimise the molecular structure at the B3LYP/6-311++G(d,p) level of theory (Becke 1993; Frisch et al. 1984) using the GAUSSIAN16 package (Frisch et al. 2016). From these calculations, we obtained values for the rotational constants, centrifugal distortion constants, and electric dipole moment components

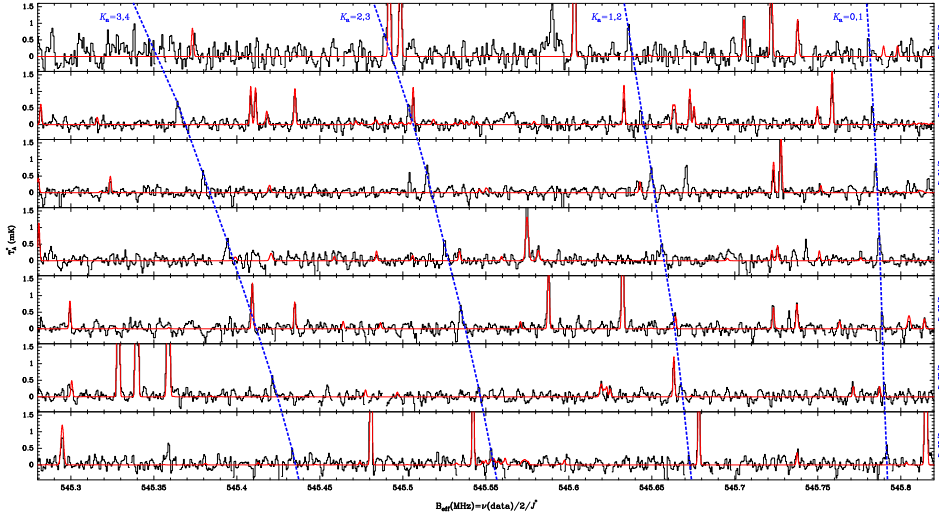


Fig. 2. Modified Loomis-Wood diagram of some of the observed lines in this work. The abscissa corresponds to the value of the rotational constant, which has been fixed in this plot to values between 545.28 and 545.82 MHz. The ordinate is the antenna temperature (corrected for atmospheric and telescope losses) in millikelvin. Each box presents the QUIJOTE data for frequencies $2 B_{\text{rot}} J^*$, where $J^* = J_u + 1/2$. The red line corresponds to the synthetic spectrum computed for TMC-1, including the rotational transitions of all molecular species detected in TMC-1. This spectrum does not contain the rotational lines discovered in this work. The rotational transitions of phenalene correspond to those connected through dashed blue lines (see text).

Table 1. Experimental and theoretical molecular constants of phenalene.

Parameter	TMC-1	Lab	TMC-1+Lab	Theory ^d
A/MHz	1108.1199(12) ^b	1108.12409(26)	1108.12404(29)	1108.6
B/MHz	1067.81464(72)	1067.81150(22)	1067.81175(23)	1067.3
C/MHz	545.85572(15)	545.85649(12)	545.85613(11)	545.6
Δ_J/Hz	19.10(63)	[19.18]	20.21(27)	19.18
Δ_{JK}/Hz	-29.5(13)	[-29.26]	-31.30(64)	-29.26
Δ_K/Hz	12.20(70)	[11.94]	13.07(38)	11.94
δ_J/Hz	[-0.237] ^c	[-0.237]	[-0.237]	-0.237
δ_K/Hz	[-20.56]	[-20.56]	[-20.56]	-20.56
N_i, N_f ^d	267,71	100,55	367,126	-
σ^2/kHz	6.2	6.6	7.4	-
$\mu_a \mu_b/D$	-	-	-	0.67,0.36
κ	0.86	0.86	0.86	0.85
$\Delta_c^f/\text{amu}\text{\AA}^2$	-3.5051(9)	-3.5060(4)	-3.5054(4)	-3.1

Notes. ^(a)Values of the rotational constants A , B , and C calculated theoretically correspond to the equilibrium rotational constants A_e , B_e , and C_e . ^(b)The uncertainties (in parentheses) are in units of the last significant digits. ^(c)Values in brackets were not determinable and were thus fixed to the theoretically calculated ones. ^(d) N_i and N_f refer to the number of distinct rotational transitions and unique transition frequencies, respectively, in the fit. ^(e)Standard root mean square deviation of the fit. ^(f)Inertial defect, $\Delta_c = I_c - I_b - I_a$. The conversion factor is 505379.1 MHz amu \AA^2 .

shown in Table 1. They agree very well with those derived from the TMC-1 data and point out that the carrier of the lines observed in TMC-1 is the PAH phenalene. The discrepancies between the experimental and calculated values of the rotational constants are smaller than 0.05%. The calculated electric dipole moment components indicate that the b -type transitions also contribute to the observed transitions. In the initial fit, we did not consider the b -type transitions; instead, by taking into account the predicted electric dipole moment components, we made a new fit of the TMC-1 data that would include these transitions. As a result, the rotational spectrum of phenalene in the Q band comprises up to four transitions: two a - and two b -type with the appropriate K_a and K_a+1 values (see Fig. A.1), collapsing up to the same frequency. The final dataset for phenalene in TMC-1 includes 71 frequencies and 267 transitions. A list of the assigned transitions with the line parameters is given in Table A.1. The final fit for the lines observed in TMC-1 provides the set of molecular constants (rotational and centrifugal), as shown in the left column of Table 1. The agreement between

the derived constants and those obtained from quantum chemical calculations indicate that phenalene is the carrier of the series of lines observed in TMC-1.

To fully confirm the astronomical discovery of phenalene in TMC-1, we carried out laboratory experiments to observe its microwave spectrum. The commercial availability of phenalene is limited; thus, we synthesised it in the laboratory. We prepared phenalene in three steps from 3-(naphthalen-1-yl)propanoic acid (see Fig. B.1), through a minor adaptation of previously published procedures (Zhao et al. 2020; Turco et al. 2023). Details of this procedure are given in Appendix B. We then measured its rotational spectrum from 2–11 GHz using a broadband chirped-pulse Fourier-transform microwave (CPFTMW) spectrometer (see details in Appendix C). In the laboratory spectrum of phenalene, we measured 55 rotational frequencies that correspond to a total of 100 rotational transitions, including a - and b -type ones. All the observed frequencies, which are available on Zenodo repository (see Sect. ‘Data availability’), were fitted using the SPFIT program (Pickett 1991) with the A -reduction of the Watson’s Hamiltonian and III' representation (Watson 1977). We only fit the values of the rotational constants, while the centrifugal distortion constants were kept fixed to the theoretical values, since the accuracy of values derived with the available data was not high enough. The values obtained from the analysis are shown in Table 1. A combined fit of the laboratory and TMC-1 data for phenalene provides the recommended molecular parameters, which are given in Table 1. As we can see, there is no doubt that phenalene is the carrier of the lines observed in TMC-1. Hence, we firmly conclude that we have detected in TMC-1 the second unsubstituted PAH after indene, which was discovered in 2021 (Cernicharo et al. 2021d).

4. Discussion

To estimate the abundance of phenalene in TMC-1, we constructed a rotational diagram, assuming its distribution as a circle with a radius of $40''$ as benzonitrile (Cernicharo et al. 2023). We obtained a rotational temperature of 7.9 ± 1.2 K, which is not far from the gas kinetic temperature of 9 K in TMC-1 (Agúndez et al. 2023), and a column density of $(2.8 \pm 1.6) \times 10^{13} \text{ cm}^{-2}$. It should be noted that these values were estimated using the theoretical dipole moment components from Table 1. The calculated line profiles are compared with the observed ones in Fig. A.1. The column density of

phenalene is somewhat larger than that of the other unsubstituted PAH detected in TMC-1, indene, for which Cernicharo et al. (2021b) derived a column density of $1.6 \times 10^{13} \text{ cm}^{-2}$. It is also interesting to note that the column density of these two pure PAHs is within the range of column densities inferred for the PAHs naphthalene, acenaphthylene, pyrene, and coronene, $(1-10) \times 10^{13} \text{ cm}^{-2}$ (McGuire et al. 2021; Cernicharo et al. 2024; Wenzel et al. 2024, 2025a,b). However, we note that the latter range has a significant uncertainty due to the conversion factor used to scale the abundance of the cyano derivative to that of the corresponding unsubstituted PAHs, where factors in the range between 5–30 are typically estimated (Cernicharo et al. 2022; Wenzel et al. 2025b; Steber et al. 2025).

It is puzzling how phenalene and the other PAHs detected in TMC-1 could have been formed at such large abundances (i.e. in the range 10^{-9} – 10^{-8}) relative to H_2 . If PAHs are formed through a bottom-up mechanism, we can consider the plausible chemical reactions that would be able to synthesise phenalene from smaller cycles. Neutral-neutral reactions between smaller PAHs and reactive radicals could, in principle, do the job. If exothermic and barrierless, these reactions commonly occur with H atom elimination. There are several potentially interesting reactions to consider, such as those between naphthalene and propargyl radical ($\text{C}_{10}\text{H}_8 + \text{C}_3\text{H}_3$), indene (C_9H_8) and the C_4H_3 radical, and acenaphthylene (C_{12}H_8) and the CH_3 radical, all of which involve reactants which are known or expected to be abundant in TMC-1. However, these reactions are calculated with the assumption that they include barriers in the channel yielding phenalene, as we show using our own quantum chemical calculations (Appendix D). Another bottom-up route could be provided by ion-neutral reactions able to form protonated phenalene ($\text{C}_{13}\text{H}_{11}^+$), the dissociative recombination of which with electrons could yield phenalene. An investigation of the dissociation channels of $\text{C}_{13}\text{H}_{11}^+$ using automatic reaction discovery methods (Maeda et al. 2013, 2023a) offers a promising pathway via the reaction of acenaphthylene C_{12}H_8 with the methyl cation CH_3^+ . This is an exothermic and barrierless reaction (Appendix D), following the emission of a photon (i.e. $\text{C}_{12}\text{H}_8 + \text{CH}_3^+ \rightarrow \text{C}_{13}\text{H}_{11}^+ + h\nu$) and a subsequent dissociative recombination (as mentioned above) to form phenalene. This highlights the importance of reconsidering ion-neutral reactions, including radiative associations in the formation of PAHs in the ISM.

5. Conclusions

In the present work, we report the detection of the second unsubstituted PAH in TMC-1 to date, namely, phenalene. The discovery of this PAH is based on the observation of 71 lines in our line survey QUIJOTE and supported by laboratory rotational spectroscopy experiments. The derived column density of phenalene is similar to those found for other PAHs in the same source. The chemistry of PAHs in the ISM is still not understood, especially for medium-sized PAHs such as phenalene. Our preliminary results for this molecule suggest that the ion-molecule chemistry could play a more significant role than previously expected.

Data availability

The data underlying this article are available on Zenodo repository (<https://doi.org/10.5281/zenodo.16911003>). Data comprise the line parameters toward TMC-1 (full Table A.1) and the TMC-1 and laboratory measured frequencies for phenalene.

Acknowledgements. This work was based on observations carried out with the Yebes 40m telescope (projects 19A003, 20A014, 20D023, 21A011, 21D005,

and 23A024) which is operated by the IGN, MITMA. We acknowledge funding support from MICIU through grants PID2019-106110GB-I00, PID2019-106235GB-I00, PID2021-125015NB-I00, PID2022-137980NB-I00, PID2022-139933NB-I00, and PID2023-147545NB-I00. C.P. thanks the ERC for the CoG HydroChiral (Grant Agreement No 101124939). C.P., A.L.S. and A.L. also thank funding from JCyL, Grant INFRARED IR3032-UVA13. D.V. and D.P. thank Xunta de Galicia and ERDF for Grant ED431G 2023/03. G.M. and A.L.S. acknowledge the support of the grants RYC2022-035442-I and RYC2022-037922-I, respectively, funded by MICIU/AEI/10.13039/501100011033 and ESF+. G.M. thanks support from project 20245AT016 (Proyectos Intramurales CSIC).

References

- Agúndez, M., Cabezas, C., Tercero, B., et al. 2021, *A&A*, 647, L10
 Agúndez, M., Marcelino, N., Cabezas, C., et al. 2022, *A&A*, 657, A96
 Agúndez, M., Marcelino, N., Tercero, B., et al. 2023, *A&A*, 677, A106
 Allamandola, L. J., Tielens, A. G. G. M., & Barker, J. R. 1985, *ApJ*, 290, L25
 Bannwarth, C., Ehlert, S., & Grimme, S. 2019, *J. Chem. Theory Comput.*, 15, 1652
 Becke, A. D. 1993, *J. Chem. Phys.*, 98, 1372
 Boudjouk, P., & Johnson, P. D. 1978, *J. Org. Chem.*, 43, 3979
 Bull, J. N., Subramani, A., Liu, C., et al. 2025, *Phys. Rev. Lett.*, 134, 228002
 Burkhardt, A. M., Lee, K. L. K., Changala, P. B., et al. 2021a, *ApJ*, 913, L18
 Burkhardt, A. M., Loomis, R. A., Shingledecker, C. N., et al. 2021b, *Nat. Astron.*, 5, 181
 Byrne, A. N., Xue, C., Van Voorhis, T., & McGuire, B. A. 2024, *PCCP*, 26, 26734
 Caldeweyher, E., Ehlert, S., Hansen, A., et al. 2019, *PCCP*, 150, 154122
 Cernicharo, J. 2012, in *European Conference on Laboratory Astrophysics*, eds. C. Stehlé, C. Joblin, & L. d'Hendecourt, 58, 251 EAS Publ. Ser.
 Cernicharo, J., Marcelino, N., Agúndez, M., et al. 2020, *A&A*, 642, L8
 Cernicharo, J., Agúndez, M., Kaiser, R., et al. 2021a, *A&A*, 652, L9
 Cernicharo, J., Agúndez, M., Cabezas, C., et al. 2021b, *A&A*, 649, L15
 Cernicharo, J., Agúndez, M., Kaiser, R. I., et al. 2021c, *A&A*, 655, L1
 Cernicharo, J., Agúndez, M., Cabezas, C., et al. 2021d, *A&A*, 647, L2
 Cernicharo, J., Fuentetaja, R., Agúndez, M., et al. 2022, *A&A*, 663, L9
 Cernicharo, J., Tercero, B., Marcelino, N., et al. 2023, *A&A*, 674, L4
 Cernicharo, J., Cabezas, C., Fuentetaja, R., et al. 2024, *A&A*, 690, L13
 Fossé, D., Cernicharo, J., Gerin, M., & Cox, P. 2001, *ApJ*, 552, 168
 Frisch, M. J., et al. 2016, Gaussian 16 Revision A.03
 Frisch, M. J., Pople, J. A., & Binkley, J. S. 1984, *J. Chem. Phys.*, 80, 3265
 Gordy, W., & Cook, R. 1984, *Microwave Molecular Spectra* (New York: Wiley)
 Léger, A., & Puget, J. L. 1984, *A&A*, 500, 279
 Maeda, S., Ohno, K., & Morokuma, K. 2013, *PCCP*, 15, 3683
 Maeda, S., Harabuchi, Y., Hayashi, H., & Mita, T. 2023a, *Annu. Rev. Phys. Chem.*, 74, 287
 Maeda, S., Harabuchi, Y., Sumiya, Y., et al. 2023b, *GRRM23*, <https://global.hpc.co.jp/products/grrm23/>
 Mardirossian, N., & Head-Gordon, M. 2016, *J. Chem. Phys.*, 144, 214110
 McGuire, B. A., Burkhardt, A. M., Kalenskii, S., et al. 2018, *Science*, 359, 202
 McGuire, B. A., Loomis, R. A., Burkhardt, A. M., et al. 2021, *Science*, 371, 1265
 McNaughton, D., Jahn, M. K., Travers, M. J., et al. 2018, *MNRAS*, 476, 52678
 Müller, H. S. P., Schlöder, F., Stutzki, J., & Winnewisser, G. 2005, *J. Mol. Struct.*, 742, 215
 Najibi, A., & Goerigk, L. 2020, *J. Comput. Chem.*, 41, 2562
 Neese, F. 2022, *WIREs Comput. Mol. Sci.*, 12, e1606
 Pérez, C., Lobsiger, S., Seifert, N. A., et al. 2013, *Chem. Phys. Lett.*, 571, 1
 Pety, J., Teyssier, D., Fossé, D., et al. 2005, *A&A*, 435, 885
 Pickett, H. M. 1991, *J. Mol. Spectr.*, 148, 371
 Pickett, H. M., Poynter, R. L., Cohen, E. A., et al. 1998, *J. Quant. Spectrosc. Radiat. Transfer*, 60, 883
 Sita, M. L., Changala, P. B., Xue, C., et al. 2022, *ApJ*, 938, L12
 Steber, A. L., Janeiro, J., Cabezas, C., et al. 2025, *A&A*, 700, A281
 Tercero, F., López-Pérez, J. A., Gallego, J. D., et al. 2021, *A&A*, 645, A37
 Thorwirth, S., Theulé, P., Gottlieb, C. A., et al. 2007, *ApJ*, 662, 1309
 Tielens, A. G. G. M. 2008, *Annu. Rev. Astron. Astrophys.*, 46, 289
 Turco, E., Bernhardt, A., Krane, N., et al. 2023, *JACS Au*, 3, 1358
 Watson, J. K. G. 1977, in *Vibration Spectra and Structure*, ed. J. Durig (Amsterdam: Elsevier), 6, 1
 Weigend, F., & Ahlrichs, R. 2005, *PCCP*, 7, 3297
 Wenzel, G., Cooke, I. R., Changala, P. B., et al. 2024, *Science*, 386, 810
 Wenzel, G., Speak, T. H., Changala, P. B., et al. 2025a, *Nat. Astron.*, 9, 262
 Wenzel, G., Gong, S., Xue, C., et al. 2025b, *ApJ*, 984, L36
 Zhao, L., Kaiser, R. I., Lu, W., et al. 2020, *PCCP*, 22, 15381
 Zhen, J., Castellanos, P., Paardekooper, D. M., et al. 2014, *ApJ*, 797, L30
 Zheng, J., Xu, X., & Truhlar, D. G. 2011, *Theor. Chem. Acc.*, 128, 295

Table A.1. Observed line parameters of phenalene in TMC-1.^a

Transition ^b	ν_{obs}^c (MHz)	$\int T_A^* dv^d$ (mK km s ⁻¹)	$\Delta\nu^e$ (km s ⁻¹)	T_A^f (mK)
27 _{β,26} -26 _{β,25}	31101.252±0.010	0.90±0.32	0.81±0.35	1.03±0.21
28 _{α,28} -27 _{α,27}	31109.488±0.010	0.39±0.19	0.51±0.24	0.70±0.19
19 _{λ,9} -18 _{λ,8}	32129.188±0.010	0.33±0.10	0.62±0.30	0.50±0.11
21 _{ι,13} -20 _{ι,12}	32137.269±0.010	0.36±0.12	0.72±0.24	0.47±0.09
22 _{θ,15} -21 _{θ,14}	32144.436±0.010	0.91±0.11	1.20±0.21	0.71±0.09
23 _{η,17} -22 _{η,16}	32152.173±0.010	0.51±0.11	0.90±0.21	0.53±0.08
24 _{ζ,19} -23 _{ζ,18}	32160.171±0.010	0.41±0.12	0.93±0.37	0.41±0.07
25 _{ϵ,21} -24 _{ϵ,20}	32168.288±0.010	0.35±0.10	0.71±0.22	0.46±0.08
26 _{δ,23} -25 _{δ,22}	32176.490±0.010	0.44±0.07	0.76±0.15	0.53±0.11
27 _{γ,25} -26 _{γ,24}	32184.712±0.010	0.49±0.09	0.74±0.15	0.62±0.12
28 _{β,27} -27 _{β,26}	32192.950±0.010	0.45±0.12	0.69±0.21	0.60±0.10
29 _{α,29} -28 _{α,28}	32201.186±0.010	0.36±0.12	0.51±0.28	0.67±0.09
21 _{κ,12} -20 _{κ,11}	33222.247±0.010	0.26±0.07	0.58±0.18	0.42±0.10
22 _{ι,14} -21 _{ι,13}	33228.623±0.010	0.56±0.11	0.95±0.21	0.56±0.08
27 _{δ,24} -26 _{δ,23}	33268.165±0.010	0.55±0.09	0.79±0.15	0.66±0.09
28 _{γ,26} -27 _{γ,25}	33276.398±0.010	0.79±0.09	0.93±0.12	0.80±0.10

Notes. ^(a) The full contents of this table can be found in electronic form at Zenodo (see Section 5). All uncertainties correspond to 1σ . ^(b) Each frequency in the second column is assigned to four rotational transitions: two *a*- and two *b*-type ones. Labels $\alpha, \beta, \gamma, \delta, \epsilon, \zeta, \eta, \theta, \iota, \kappa, \lambda$ correspond to $K_a=0,1, K_a=1,2, K_a=2,3, K_a=3,4, K_a=4,5, K_a=5,6, K_a=6,7, K_a=7,8, K_a=8,9, K_a=9,10$, and $K_a=10,11$, respectively, for each quartet of lines. As an example, the line at 31101.252 MHz is assigned to the quartet of lines 27 _{β ,26}-26 _{β ,25}, which means to 27_{0,26}-26_{0,25}, 27_{0,26}-26_{1,25}, 27_{1,26}-26_{0,25} and 27_{1,26}-26_{1,25} transitions. ^(c) Measured frequency assuming a v_{LSR} of 5.83 km s⁻¹ for TMC-1 (Cernicharo et al. 2020). ^(d) Integrated line intensity (in mK km s⁻¹). ^(e) Linewidth at half intensity derived by fitting a Gaussian function to the observed line profile (in km s⁻¹). ^(f) Antenna temperature (in milliKelvin).

Appendix A: Line parameters of phenalene

Line parameters for all observed transitions with the Yebes 40m radio telescope were derived by fitting a Gaussian line profile to them using the GILDAS package. A velocity range of ± 50 km s⁻¹ around each feature was considered for the fit after a polynomial baseline was removed. Negative features in the folding of the frequency switching data were blanked before baseline removal. A view of some of the transitions of phenalene is given in Fig. A.1.

Appendix B: Synthesis of phenalene

B.1. General synthetic methods

Reactions were carried out under argon using oven-dried glassware. THF and CH₂Cl₂ were obtained from a MSBraun SPS-800 Solvent Purification System. Other commercial reagents were purchased from Sigma-Aldrich or BLD-Pharm and used without further purification. 1*H*-phenalene was synthesised (Fig. B.1) following reported procedures with minor modifications (Zhao et al. 2020; Turco et al. 2023). Thin-Layer Chromatography (TLC) was performed on Merck silica gel 60 F254 and chromatograms were visualised with UV Light (254 nm and 360 nm). Column chromatography was performed on Merck silica gel 60 (ASTM 40-60 μm). NMR spectra were recorded at 500 MHz and 125 MHz for ¹H and ¹³C, respectively (Bruker DRX-500). Gas Chromatography/Mass Spectrometry (GC/MS) analysis were conducted on a HP 5973 INERT coupled to Agilent HP-5MS. Atmospheric pressure chemical ionisation (APCI) high-resolution mass spectrometry spectra were obtained on a Bruker Microtof using a direct inlet probe (DIP) for the sample introduction.

B.2. Experimental procedures and characterisation data

B.2.1. Synthesis of 2,3-dihydro-1*H*-phenalen-1-one

A mixture of 3-(naphthalen-1-yl)propanoic acid (506 mg, 2.42 mmol) and SOCl₂ (4 mL) was heated to 80°C for 1 h. The volatiles were removed under vacuum and the resulting oily crude was dissolved in dry CH₂Cl₂ (2 mL) and it was added dropwise to a solution of AlCl₃ (759 mg, 5.70 mmol) in dry CH₂Cl₂ (9 mL) at -20°C. The mixture was stirred for 30 min and it was poured into ice. Layers were separated and the aqueous phase was extracted with CH₂Cl₂. The organics were dried over anhydrous Na₂SO₄, the solvent was removed by rotary evaporation and the crude was purified by column chromatography (SiO₂, hexane/AcOEt 4:1) to obtain 2,3-dihydro-1*H*-phenalen-1-one as a colorless solid (332 mg, 1.82 mmol, 75%). The spectroscopic data were identical to those reported in the literature (Turco et al. 2023).

¹H-NMR (500 MHz, Chloroform-*d*) δ : 8.19 (dd, $J = 7.2, 1.3$ Hz, 1H), 8.06 (dd, $J = 8.1, 1.3$ Hz, 1H), 7.78 (dd, $J = 8.3, 1.2$ Hz, 1H), 7.58 (dd, $J = 8.2, 7.2$ Hz, 1H), 7.51 – 7.40 (m, 2H), 3.41 (m, 2H), 2.99-2.94 (m, 2H). ¹³C-NMR-DEPT (126 MHz, Chloroform-*d*) δ : 198.54 (C), 134.10 (CH), 133.45 (C), 133.28 (C), 131.68 (C), 129.86 (C), 126.32 (2xCH), 125.72 (CH), 125.59 (CH), 125.09 (CH), 38.56 (CH₂), 28.60 (CH₂) ppm. Spectra shown in Fig. B.2.

B.2.2. Synthesis of 2,3-dihydro-1*H*-phenalen-1-ol

First, 2,3-dihydro-1*H*-phenalen-1-one (311 mg, 1.82 mmol) was dissolved in a mixture 5:3 of dry MeOH/THF (8 mL) and NaBH₄ (137 mg, 3.64 mmol) was added at 0°C in one portion. The mixture was stirred for 5 min and then it was allowed to warm up to room temperature and stirred for 30 min. Water and AcOEt were added, layers were separated and the aqueous phase was extracted with AcOEt. The organics were dried over anhydrous Na₂SO₄ and solvents were removed by rotary evaporation to afford pure 2,3-dihydro-1*H*-phenalen-1-ol as a colorless solid (314 mg, 1.70 mmol, 94%). Spectroscopic data were identical to those reported in the literature (Turco et al. 2023).

¹H-NMR (500 MHz, Chloroform-*d*) δ : 7.81 (d, $J = 8.2$ Hz, 1H), 7.73 (d, $J = 8.2$ Hz, 1H), 7.55 (d, $J = 7.0$ Hz, 1H), 7.48 (d, $J = 7.6$ Hz, 1H), 7.46-7.42 (m, 1H), 7.31 (d, $J = 7.0$ Hz, 1H), 5.07 (dd, $J = 6.8, 3.8$ Hz, 1H), 3.40-3.04 (m, 2H), 2.18 (m, 2H). ¹³C-NMR-DEPT (126 MHz, Chloroform-*d*) δ : 137.53 (C), 135.19 (C), 133.71 (C), 128.79 (C), 128.05 (CH), 125.96 (CH), 125.73 (CH), 125.66 (CH), 124.43 (CH), 123.54 (CH), 69.40 (CH), 31.39 (CH₂), 26.37 (CH₂) ppm. Spectra shown in Fig. B.3.

B.2.3. Synthesis of 1*H*-phenalene

A catalytic amount of p-TsOH was added to a solution of 2,3-dihydro-1*H*-phenalen-1-ol (314 mg, 1.70 mmol) in toluene (10 mL) with 4 Å sieves and the mixture was heated to 110°C for 30 min. Then it was cooled to room temperature and the solvent was removed. The crude was purified by flash column chromatography (SiO₂, hexane) to obtain 1*H*-phenalene as a colorless solid (108 mg, 0.65 mmol, 38%). Spectroscopic data were identical to those reported in the literature (Zhao et al. 2020; Turco et al. 2023).

¹H-NMR (300 MHz, Chloroform-*d*) δ : 7.59 – 7.50 (m, 2H), 7.36 (t, $J = 7.6$ Hz, 1H), 7.31 – 7.22 (m, 2H), 6.98 (d, $J = 6.9$ Hz, 1H), 6.60 (dt, $J = 9.9, 2.3$ Hz, 1H), 6.05 (dt, $J =$

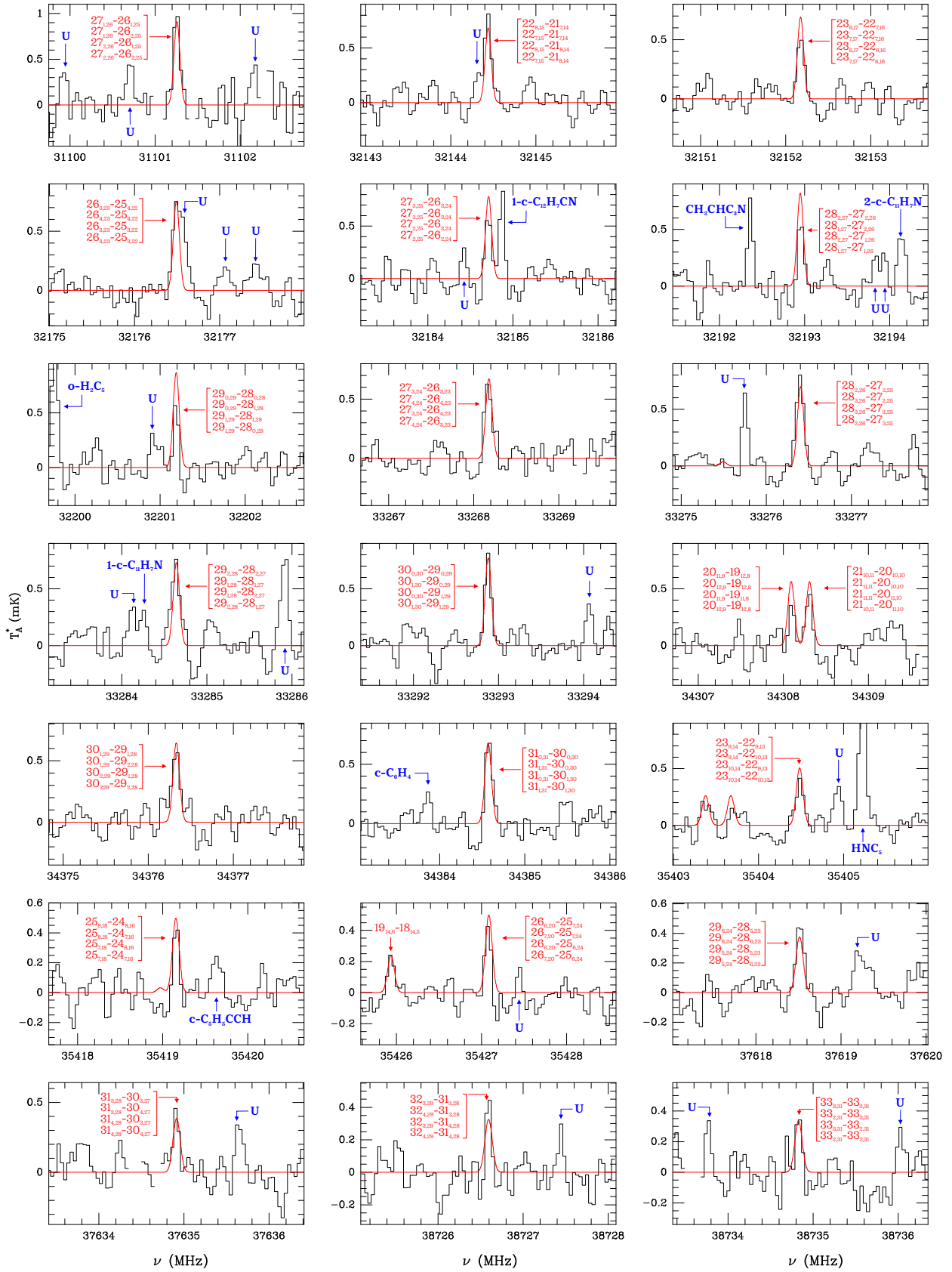
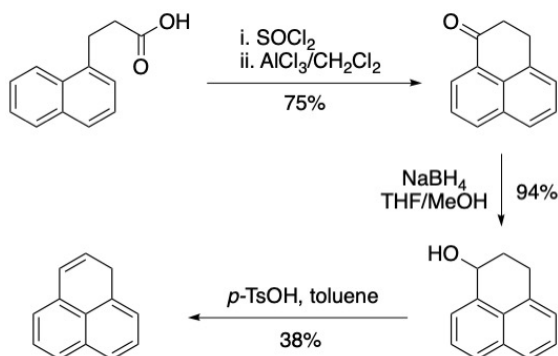
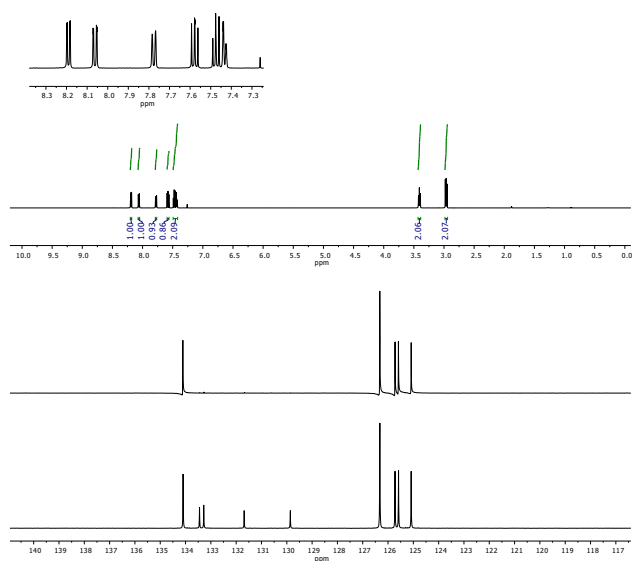
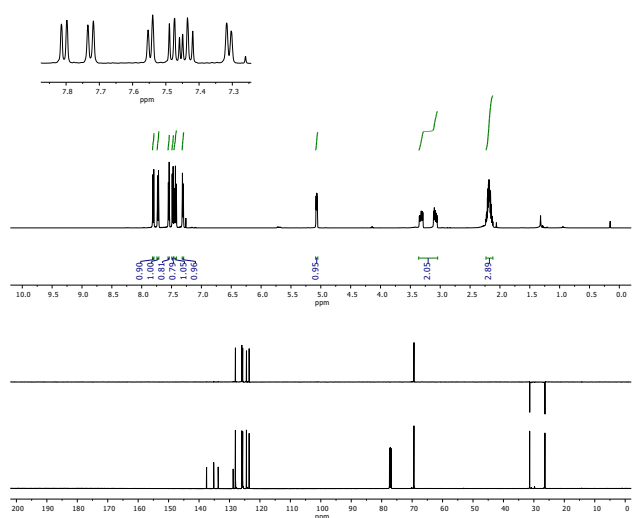
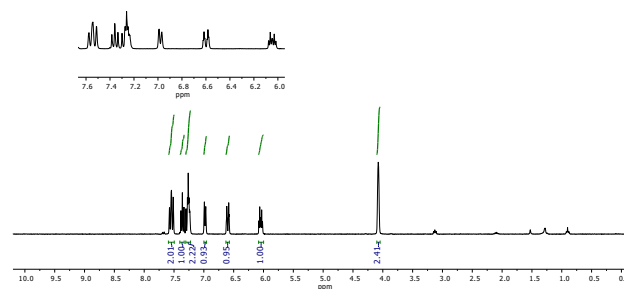


Fig. A.1. Selection of observed lines of phenalene in TMC-1 from the QUIJOTE line survey (black histogram) and synthetic spectra (red curve) calculated adopting a column density of $2.8 \times 10^{13} \text{ cm}^{-2}$. Blanked channels correspond to negative features produced in the folding of the frequency switching data. The lines are indicated by arrows and their quantum numbers are depicted for each feature. Other lines from molecules previously studied or unknown features are indicated in blue. The abscissa corresponds to the rest frequency assuming a local standard of rest velocity of 5.83 km s^{-1} . The ordinate is the antenna temperature in millikelvin.

Fig. B.1. Synthesis of 1*H*-phenalene.Fig. B.2. ^1H and ^{13}C -NMR spectra of 2,3-dihydro-1*H*-phenalene-1-one.Fig. B.3. ^1H and ^{13}C -NMR spectra of 2,3-dihydro-1*H*-phenalene-1-ol.

9.9, 4.1 Hz, 1H), 4.08 (bs, 2H). Mp 80-81°C (Lit. 83-84 °C) (Boudjouk & Johnson 1978). Spectra are shown in Fig. B.4.

Fig. B.4. ^1H spectrum of 1*H*-phenalene.

Appendix C: Laboratory rotational spectroscopy measurements

The experimental setup employed to measure the rotational spectra of phenalene consists of broadband chirped-pulse Fourier-transform microwave (CPFTMW) spectrometer working from 2-18 GHz. The design is largely based on the original design by Pérez et al. (2013) with some modifications to allow for direct excitation-detection of the whole 16 GHz bandwidth. The excitation pulse, ranging from 1 to 9 GHz, is directly generated using an arbitrary waveform generator (Tektronix AWG 70002A, 25 GS/s). This pulse is pre-amplified and frequency-doubled to produce a 4 μs pulse within the 2-18 GHz range. Subsequently, the pulse is amplified using a solid-state amplifier (SSA Qorvo QPB0220N, 54 dBm output power) that operates over the entire frequency range. The sample phenalene (see Appendix B for description) was placed in a reservoir near the valve orifice and heated to $\sim 80^\circ\text{C}$ to generate sufficient vapor pressure. These samples were then seeded into a supersonic expansion by mixing with 3.5 bar neon before being expanded into a vacuum chamber. The gas ensemble interacted with the amplified chirped excitation pulse, inducing a macroscopic dipole moment in all polar species within the pulse. The molecular emission was amplified by a 2-18 GHz low-noise amplifier (Miteq LNAS-55-01001800-22-10P) and collected for 20 μs in the time domain as a free-induction decay using a fast oscilloscope (Tektronix DPO 73304DX, 100 GS/s). For each gas pulse, 20 chirped pulses and a repetition rate of 4 Hz were used, giving an overall repetition rate of 80 Hz. The recorded waveform was then Fourier-transformed to obtain the final frequency-domain spectrum (see Fig. C.1).

Appendix D: Initial exploration of ISM compatible formation routes for phenalene

To support our conclusions regarding the chemistry of phenalene in the ISM, we performed a preliminary exploration of possible formation routes for it using quantum chemical calculations. As briefly mentioned in the main text, we focused on the formation of phenalene via neutral-neutral reactions involving already detected PAHs: naphthalene (C_{10}H_8), indene (C_9H_8), and acenaphthylene (C_{12}H_8), reacting with the arithmetically compatible radicals C_3H_3 (linear), C_4H_3 , and CH_3 to form $\text{C}_{13}\text{H}_{10} + \text{H}$. These reactions were investigated using the ORCA 6.0 program (Neese 2022) at the $\omega\text{B97M-D4/ma-def2-TZVP}$ level of theory (Mardirossian & Head-Gordon 2016; Najibi & Goerigk 2020; Caldeweyher et al. 2019; Weigend & Ahlrichs 2005; Zheng et al. 2011). All inequivalent positions of C_{10}H_8 , C_9H_8 , and C_{12}H_8 were sampled. Although interesting chemical pathways emerged from our investigation, such as the formation of triangular adducts with several of the unsaturated PAH backbones, all the reactions we explored exhibited activation

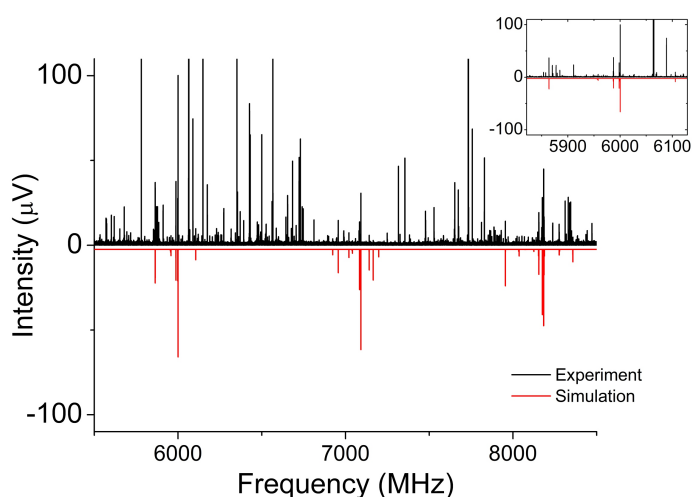


Fig. C.1. Inset of the recorded spectrum arising from gas-phase phenalene. The upper trace is the experimental spectrum, and the red trace is the simulated spectrum derived from the fitted rotational parameters at 1 K for phenalene.

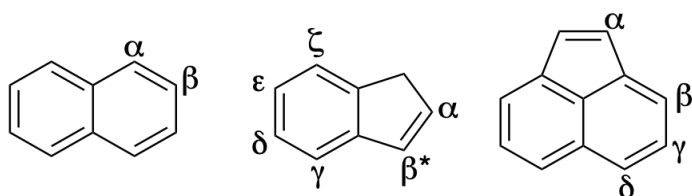


Fig. D.1. Naphthalene ($C_{10}H_8$), indene (C_9H_8) and acenaphthylene ($C_{12}H_{10}$) structures along with the symmetry inequivalent positions for reactions with radicals, see text. We note that for indene α and β positions yield the same adduct (triangular).

Table D.1. Activation energies for neutral-neutral reactions considered in this work, in kJ mol^{-1} with labels from Figure D.1. All energies are ZPE-corrected.

Position	ΔU_a (kJ mol^{-1})
$C_{10}H_8 + C_3H_3$	
α	50.8
β	61.6
$C_9H_8 + C_4H_3$	
α^a	34.1
γ	61.6
δ	65.3
ϵ	59.0
ζ	61.5
$C_{12}H_8 + CH_3$	
α	22.8
β	32.3
γ	43.8
δ	29.9

Notes. Reference energies are calculated from the separated reactants
^(a) α and β positioning of C_4H_3 yield the same adduct.

energies that rule them out as viable low-temperature bottom-up formation routes. A summary of the sampled reactions is given in Figure D.1 and Table D.1.

In addition to neutral-neutral reactions, we also explored the formation of protonated phenalene ($C_{13}H_{11}^+$), which can

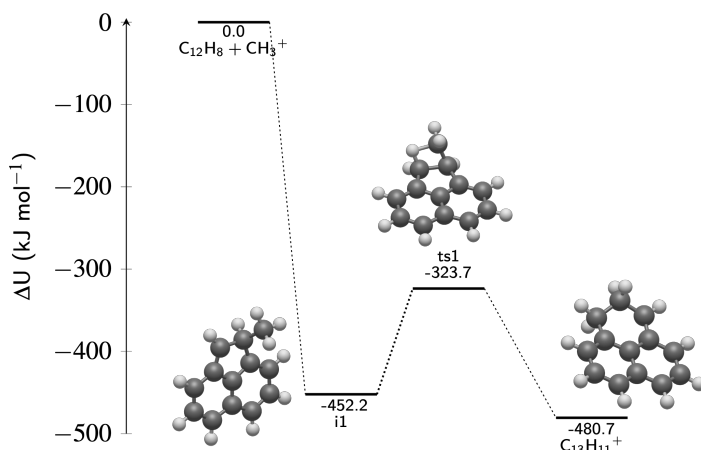
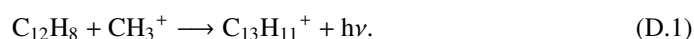


Fig. D.2. Proposed simplified scheme for the formation of $C_{13}H_{11}^+$

yield neutral phenalene via dissociative recombination, e.g., $C_{13}H_{11}^+ + e^- \rightarrow C_{13}H_{10} + H$. However, ion-molecule reactivity is generally less intuitive. To identify viable reaction pathways, we performed a computational retrosynthetic analysis using the single-component artificial force induced reaction (SC-AFIR) method, as implemented in the GRRM23 package (Maeda et al. 2013, 2023a,b), interfaced with ORCA. The calculations employed the GFN2-xTB semiempirical Hamiltonian (Bannwarth et al. 2019) and were initiated from the $C_{13}H_{11}^+$ structure, considering protonation of phenalene adjacent to the CH_2 group. The choice of protonation site was of limited importance, as hydrogen migration emerged as a common pathway in our searches. We conducted six SC-AFIR runs with different model collision energies (400, 500, 750 kJ mol^{-1}), including both global and local searches. The lowest energy search yielded 1245 equilibrium structures and 28 dissociation channels, with comparable results obtained in the replicate runs. Most dissociation pathways involved high-energy, non-viable processes. However, the search also revealed a barrierless and highly exothermic channel involving acenaphthylene ($C_{12}H_8$; Cernicharo et al. 2024), suggesting a potentially astrochemically relevant route:



The viability of the proposed reaction pathway depends on several conditions that were not addressed in this work and are deferred to a future chemical characterisation of these PAHs. While the efficiency of radiative association (Reaction D.1) is influenced by multiple factors, PAHs represent a favorable case. These relatively large molecules possess deep potential wells and numerous low-energy vibrational modes, which facilitate the dissipation of excess chemical energy through infrared radiation. A recent study on the indenyl cation ($C_9H_7^+$) by Bull et al. (2025) demonstrates efficient internal relaxation via recurrent fluorescence, suggesting that this mechanism could play an even more prominent role in larger cationic PAHs, such as $C_{13}H_{11}^+$. A simplified scheme of the DFT-refined stationary points for the reaction excluding potential bimolecular or competing channels of Reaction D.1 is presented in Figure D.2.